Research Center MATHEON
Mathematics for Key Technologies

Transient pulse compression at a group velocity horizon

Ihar Babushkin **Shalva Amiranashvili** **Carsten Brée**

Uwe Morgner **Günter Steinmeyer** **Ayhan Demircan**

Preprint

MATHEON **preprint**
http://opus4.kobv.de/opus4-matheon

Preprint **March 2016**

1 Introduction

The study and generation of light pulses that encompass only a few cycles of the electric field is a major topic in ultrafast optics, and nowadays pulses with durations of a few femtoseconds can be generated in a wide spectral range. Different laser technologies, such as chirped pulse amplification, filament self-compression, or optical parametric amplification provide nearly single-cycle pulses from the ultraviolet to the THz regime. While Ti:sapphire and its harmonics conveniently offer fairly direct schemes toward ultrashort pulses from the near infrared well into the ultraviolet, the mid-infrared (wavelength 2–25 μm) is a notoriously challenging range for direct laser-based schemes. Optical parametric schemes offer a convenient alternative, but require carefully designed phase-matching ranges and are difficult to implement. Here we explore a different path toward few-cycle pulse generation in the mid-infrared at nanojoule pulse energies. Our method follows up on Ref. [1], where a widely tunable compression scheme for pedestal-free few-cycle pulses has first been proposed. This approach requires input pulses that are tailored to fiber dispersion characteristics. Here we explore how to increase the practicality of this method by introducing the chirp of one of the input pulses as an additional control parameter. This waveform control strongly resembles the function of an optical transistor [2], yet with the decisive difference that the control pulse induces changes of compression factor and pulse duration rather than of amplitude.

This scheme inherently relies on cross-phase modulation (XPM) between two group-velocity matched pulses at different wavelengths [2]. In fact, this condition is automatically met in fibers in the vicinity of the zero dispersion wavelength, where a soliton with a particular wavelength always co-propagates with dispersive radiation at equal group velocity. In this situation, the soliton may exhibit an intensity that is high enough for creating a refractive index barrier for the dispersive wave. Cross-phase modulation then modifies the group velocity of the dispersive wave such that an effective temporal lock of the soliton and the dispersive wave is established. This collision process may alternatively be understood as scattering or reflection of the dispersive radiation at the soliton [3, 4, 5]. This kind of XPM process is known as the optical push broom effect [6] or the optical event horizon [8, 9] and has an analogy in many nonlinear wave systems, e.g., in fluid dynamics [11]. Moreover, it appears naturally in the supercontinuum generation by soliton fission [12, 13, 14]. Direct experimental verification of the reflection process at the induced refractive index barrier can be found in Refs. [8, 10, 7, 20, 15].

Given energy conservation, the collision process inevitably induces a frequency shift of both pulses [5], which enables mutual manipulation of optical pulses [2, 16, 17, 18, 19, 20]. In particular, the induced soliton center frequency shift can be efficiently exploited, e.g., by an induced blue shift of the solitons, which, in turn, leads to adiabatic soliton compression. This shift enables the generation of few-cycle pulses [1]. Nevertheless, given a certain dispersion profile of a fiber, practical exploitation of the compression always requires the generation of a soliton and a dispersive wave with center wavelengths and durations tailored to the particular situation. Some minor adjustment is only possible by changing the initial delay between the pulses.

Very recently, this novel type of soliton compression via interaction with the dispersive wave was experimentally demonstrated [23], yet with pulse duration that seem far from exploiting the full potential of the method. This experimental verification employed two coherent pulses at ≈ 600 and 800 nm and a fiber with zero-dispersion wavelength at ≈ 700 nm. The dispersive wave was deduced from the 800 nm pulses by an optical parametric oscillator with subsequent

frequency doubling. Larger wavelength separations can also be obtained from parametric generation schemes with reverted roles, i.e., the pump wavelength lies in the normal dispersion scheme of the fiber, and either the signal or even the idler wavelength is launched into the fiber in the anomalous dispersion range. In the following, we have chosen a wavelength combination that could, in principle, be deduced from a frequency-doubled ytterbium pump laser, using additional optical parametric amplification with the idler set to 2.2 μm wavelength. The necessary pulse durations in the visible should be immediately obtainable from existing ytterbium oscillators and amplifiers by simple frequency doubling schemes. However, pulse preparation in the infrared may require additional compression efforts. One of the limiting factors in our scheme is the presence of Raman self-frequency shift, which cannot be compensated by control of the dispersive wave delay and duration. As we show below, additional control can be obtained by varying the chirp of the dispersive wave, which acts as the control pulse. Let us remark that suitable chirps can be introduced intentionally in experiments by wedge or prism pairs. Moreover, small residual chirps may also be experimentally unavoidable in the preceding pulse preparation schemes, and the question may arise what values can be tolerated here without preventing compression.

2 Adjustable pulse compression at a group-velocity horizon

To model collision and scattering of two co-propagating pulses with considerably different carrier frequencies, we describe the electric field $E(z,t)$ in terms of the so-called analytic signal $\mathcal{E}(z,t) = \frac{1}{\pi}\int_0^\infty E(z,\omega)e^{-i\omega t}d\omega$, where $E(z,\omega)$ is the usual spectral component of the field $E(z,t) = \frac{1}{2\pi}\int_{-\infty}^\infty E(z,\omega)e^{-i\omega t}d\omega$. Here, $E(z,t)$ is real-valued and contains both positive and negative frequencies, whereas $\mathcal{E}(z,t)$ is complex-valued and contains only positive frequencies [28, 29]. This formalism does not require definition of a carrier frequency and is independent on the slowly-varying envelope approximation. The corresponding propagation equation is bidirectional [30], and its unidirectional version reads

$$\partial_z\mathcal{E} + \hat{\beta}\mathcal{E} + \frac{n_2}{c}\partial_t(f_K|\mathcal{E}|^2\mathcal{E} + f_R\mathcal{E}\hat{h}|\mathcal{E}|^2)_+ = 0, \tag{1}$$

and is similar to the generalized nonlinear Schrödinger equation (GNLSE). The only structural difference from the GNLSE is that the negative-frequency part of the nonlinear terms like $|\mathcal{E}|^2\mathcal{E}$ is put to zero, this is indicated by the notation $(|\mathcal{E}|^2\mathcal{E})_+$.

The parameter n_2 in Eq. (1) is the nonlinear refractive index, c the speed of light, operator $\hat{\beta}$ is defined in the frequency domain by the propagation constant $\beta(\omega)$, and V is the velocity of the moving frame such that $\hat{\beta}e^{-i\omega t} = -i[\beta(\omega) - \omega/V]e^{-i\omega t}$. The parameters f_K and $f_R = 1 - f_K$ describe relative contributions of the Kerr and Raman effect, respectively, and $\hat{h}$ denotes a standard convolution with the Raman response function

$$\hat{h}|\mathcal{E}(z,t)|^2 = \int_0^\infty h(t')|\mathcal{E}(z,t-t')|^2dt',$$

where

$$h(t') = \frac{\tau_1^2+\tau_2^2}{\tau_1\tau_2^2}e^{-t'/\tau_2}\sin(t'/\tau_1).$$

The expression for $\beta(\omega)$ and the specific values of $f_{K,R}$ and $\tau_{1,2}$ are specified in [1]. The velocity V equals that of the soliton. For numerical solution of Eq. (1), we use a de-aliased

pseudo-spectral method, with the implementation of the Runge-Kutta integration scheme in the frequency domain and adaptive step-size control. Quality of the time discretization is ensured by exemplary runs with a considerably larger number of harmonics.

This approach allows investigating the interaction of two pulses at well-separated center frequencies, far away from restrictions of the slowly-varying envelope approximation, which is sometimes presupposed in similar studies. In particular, the center frequencies of the interacting waves may readily be separated by an octave or more. The capability to include arbitrary frequencies is crucial as we are mainly interested in the interaction of a fundamental soliton in the mid-IR with a dispersive wave close to the ultraviolet region. Under these circumstances, we avoid the main limitation of the compression scheme due to resonant transfer of energy from the soliton into the normal dispersion regime in the form of Cherenkov radiation [1, 13]. As Eq. (1) is not completely equivalent to the full Maxwell equations, it does not include the backward-propagating waves. Moreover, we also neglect a frequency dependence of n_2.

As a nonlinear dispersive medium we exemplarily choose an endlessly single-mode (ESM) photonic crystal fiber [24]. In terms of choice of the medium, we only require that the dispersion profile exhibit at least one zero dispersion wavelength (ZDW). Such a precondition is given in a large class of silica-based fibers, but also in other materials as, e.g., fluoride based ZBLAN fibers [25]. Moreover, adequate dispersion profiles can be found in Raman-free gas-filled hollow core photonic crystal fibers [26], where the dispersion properties can additionally be adjusted by pressure variation. Anomalous and normal branches of the corresponding group velocity dispersion profile for the ESM fiber are shown in Fig. 1(a,b) together with a suitably chosen group-velocity matched frequency combination between a soliton and a dispersive wave (fat red and blue points, respectively). The parameters are chosen to provide a compression of a fundamental soliton into the few-cycle regime. In principle, this choice enables maximum compression down to duration in the single-cycle regime. Limitations arise due to a substantial absorption of the soliton in the mid-infrared [1] or due to the generation of Cherenkov radiation [13].

For our pulse compression scheme, we have to inject two synchronized pulses $\mathcal{E}(z=0,t) = \mathcal{E}_s(t) + \mathcal{E}_d(t+t_0)$ with a time delay of $t_0 = 1000\,\mathrm{fs}$ on both sides of the ZDW. In the anomalous dispersion regime we inject a hyperbolic secant pulse

$$\mathcal{E}_s(t) = \mathcal{E}_{s0}\,\mathrm{sech}(t/t_s)e^{-i\omega_s t}, \tag{2}$$

which corresponds to an exact fundamental soliton solution of the nonlinear Schrödinger equation for the dispersion value at the center frequency ω_s. The parameters for initial field $\mathcal{E}_{s0}$ and initial pulse width t_s (corresponding to FWHM duration $T_s \approx 2.634 t_s$) are then given by

$$\sqrt{n_2}\mathcal{E}_{s0} = 0.0173, \quad t_s = 16.7\,\mathrm{fs}, \quad \frac{2\pi c}{\omega_s} = 2200\,\mathrm{nm}. \tag{3}$$

In the normal dispersion regime we inject a Gaussian-shaped pulse with similar parameters for the amplitude and pulse width, i.e.,

$$\mathcal{E}_d(t) = \mathcal{E}_{d0}\exp\left(-\frac{1+iC}{2}\frac{t^2}{t_d^2}\right)e^{-i\omega_d t}, \quad \frac{2\pi c}{\omega_d} = 542\,\mathrm{nm}. \tag{4}$$

Compared to the previous work [1], we now additionally introduce the possibility of a variable initial linear chirp in the dispersive wave, determined by the dimensionless parameter C. We note that there is no simple and generally valid relation between C and the group delay

dispersion (GDD). Assuming Gaussian pulse shapes, one can relate GDD by calculating the distance required to fully compensate the chirp in the medium via $|\beta_2| = |\beta''(\omega_d)|$ and GDD $\equiv$ $\beta_2 z = -t_d^2 C/(1+C^2)$.

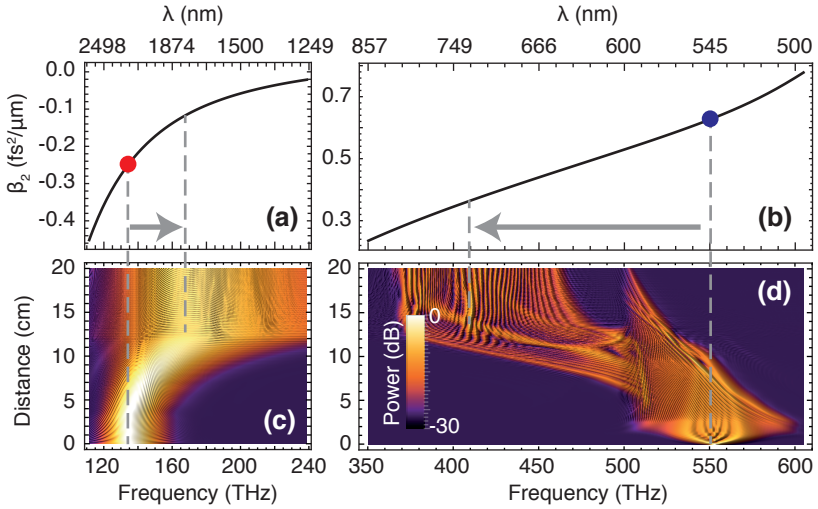

Figure 1: Collision process between a controlling dispersive wave and a soliton in the spectral domain: (a) The group velocity dispersion β_2 profile in the anomalous dispersion regime over the range of the induced soliton frequency shift. (b) The same over the frequency conversion range of the dispersive wave. (c),(d) Evolution of spectra along the fiber in the range of the (c) soliton and (d) the dispersive wave. The dashed grey lines mark the input and output center frequencies of the soliton and the dispersive wave. The red and blue dots correspond to the initial center frequency of the soliton and dispersive wave, respectively.

Let us first consider the Raman-free case. Figure 1 displays the collision behavior of the dispersive wave with the fundamental soliton in the spectral domain. For an unchirped dispersive wave ($C = 0$), we observe the following process. When parts of the dispersive wave collide with the edge of the soliton, a small mutual frequency shift between soliton and dispersive wave is induced. In our set-up the dispersive wave is injected earlier into the fiber, so that a collision occurs at the leading edge of the soliton. This process results in a blue-shift of the soliton center frequency [Fig. 1(c)] and in frequency conversion of the dispersive wave, giving rise to new red components [Fig. 1(c)]. Nearly all frequencies of the dispersive wave are converted to the range of 370 to 460 THz. Eventually, the entire spectrum of the dispersive wave is depleted. This process starts with the conversion at the initial contact between soliton and a dispersive wave segment at 600 THz and subsequently sweeps down to 500 THz. Simultaneously, the soliton frequency is up-shifted from 136 to 170 THz. The latter process is accompanied by spectral broadening from about 40 THz to more than 100 THz. This frequency shift automatically leads to a change of group velocity [Fig. 2(b)] and of group-velocity dispersion [Fig. 1(a,b)], with amount and direction depending on the dispersion profile. In this example, both pulses are shifted toward the larger group velocity.

Enabling longer interaction zones of the soliton and parts of dispersive waves, a concomitant acceleration of the soliton may be achieved. The acceleration of a soliton by interaction with the dispersive wave depicted in Fig. 2(a) is directly related to the strength of the induced frequency shift. This shift is determined by the profile of the group index $n_g = cd\beta(\omega)/d\omega$

shown in Fig. 2(b). At the same time, the change of the soliton frequency results in a shift along the group velocity dispersion β_2 profile [marked by the dashed lines in Figs. 1(a) and (c)]. For the presented set-up discussed so far, the soliton experiences an adiabatic shift towards lower values of $\beta_2 = d^2\beta(\omega)/d\omega^2$, as the β_3 component is positive in this case. A negative sign of β_3 may also appear for other dispersion profiles. For example, in fibers with two ZDWs both signs of β_3 are given, allowing decrease of β_2 with a blue frequency shift of the soliton. More importantly, for efficient compression it has to be ensured that the modulus of β_3 is high enough to enable a strong variation of β_2 along the induced soliton frequency shift.

A soliton center frequency shift toward lower dispersion values results in an adiabatic compression of the fundamental soliton [Fig. 2(d)]. This behavior is comparable to soliton compression in dispersion decreasing fibers [27], where the dispersion is manipulated by suitable prefabrication of the fiber. In our case, the change of the dispersion parameter is achieved differently by an induced frequency shift of the soliton, which, in turn, is controlled by interaction with dispersive waves. The resulting compression factor is then related to the strength of the induced frequency shift. Here lower dispersion values lead to higher peak intensities and to lower pulse width. However, the obtainable compression also depends on the initial soliton frequency and on material properties. When a soliton is injected into a range of the dispersion profile with large β_3 values, a relatively small frequency shift may already result in strong compression. For our example, this precondition is fulfilled due to the vicinity of vibrational resonances. The parameters for the simulations in Figs. 1 therefore lead to nearly purely adiabatic compression behavior, i.e., far away from the stringent limitations that were observed in the system discussed above.

3 Effect of chirp on the compression and acceleration behavior

The exact temporal frequency variation along the dispersive wave has a strong impact on group-velocity matching in the collision process. This fact suggests use of the chirp as an additional control parameter here. A carefully chosen chirp allows automatic avoidance of temporal walk-off effects due to the varying soliton frequency.

As the soliton frequency constantly increases during the entire interaction process, the frequency of the dispersive wave should constantly decrease [see Fig. 2(b)] to avoid early stagnation of the collision process. To this end a positive chirp has to be induced.

To illustrate this feature, we choose a dispersive pulse width of $t_d = 300\,\mathrm{fs}$ and an amplitude of $\mathcal{E}_d = 0.3\mathcal{E}_s$. With this setup, we performed several simulations at different chirp parameters varying from $C = -12$ to 12 (GDD ≈ -830 to $830\,\mathrm{fs}^2$). The spectral dynamics of the dispersive wave for different chirps are shown in Figs. 2 (c) and (d). Here the evolution of the spectrum of the dispersive waves is shown in comparison with that carrying a chirp of $C = 6$ (GDD $\approx 1620\,\mathrm{fs}^2$). As one can see, the interaction of a positively chirped dispersive wave with a soliton leads to a shift of frequencies interacting with the soliton, and thus a stronger acceleration of the latter, such that it arrives earlier at the fiber end. In the (t, z)-plane picture, this implication results in a stronger curvature of the soliton trajectory (similar to the case presented in Fig. 3). The soliton acceleration is accompanied by its compression due to the adiabatic frequency shift along the dispersion profile. The net effect of this compression is shown in Fig. 1(b), where we compare the peak intensities I of the soliton at the fiber end ($z = 30\,\mathrm{cm}$) for different values of the initial chirp C of the dispersive wave. Consequently, increasing the positive chirp of the dispersive wave, an immediate enhancement of the soliton

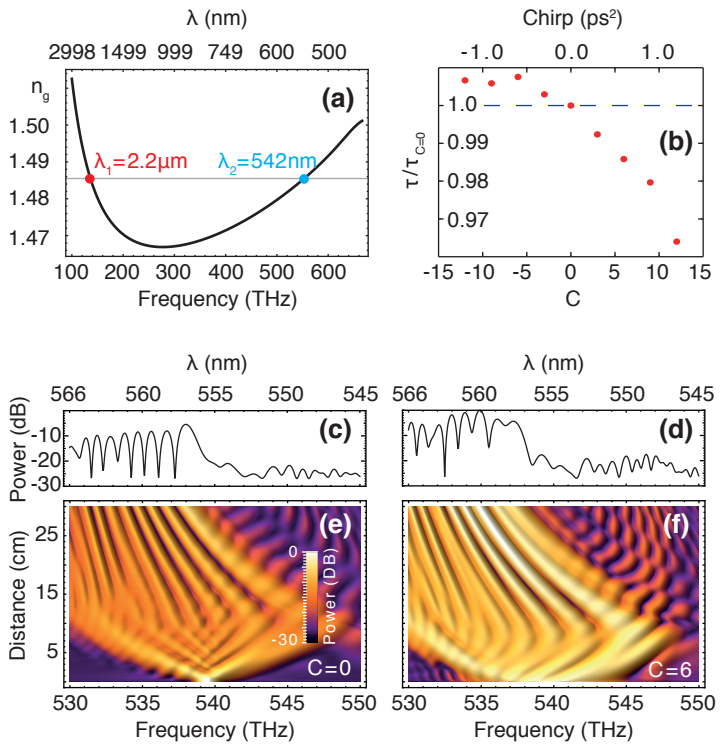

Figure 2: (a) Group index n_g of the fiber. Positions of the soliton and dispersive wave are indicated by the red and blue dots, respectively. (b) Pulse duration at the fiber output (30 cm) is shown in dependence on the dispersive wave chirp C (normalized to pulse duration for the case $C = 0$). (c–f) Details of the dispersive wave evolution in frequency range (e,f) and the output spectrum (c,d) for the chirp parameter $C = 0$ (c,e) and $C = 6$ (GDD $\approx 1620\,\mathrm{fs}^2$) (d,f) are presented. One can see the broader spectrum in (f) for $z = 0$. Dispersive waves in resonance with the soliton reach higher intensity upon further propagation.

compression mechanism results.

Also, a positive chirp makes the spectrum of the dispersive wave broader (see Fig. 2), both at the beginning of the fiber and beyond. In contrast, a negative chirp leads to spectral narrowing after a certain distance (not shown). The blue frequency components of the trailing edge of the dispersive wave can thus be adjusted to a better group velocity matching with the frequency components at the leading edge of the soliton. Thus, the reflection process at the first collision point is optimized, leading to stronger acceleration. Upon further propagation, the frequency shift of the soliton feeds on portions of the dispersive wave with suitably delayed frequency components. For obtaining a blue-shift of the soliton, suitably red-shifted segments of the dispersive wave are required at the collision points. Otherwise, group-velocity matching cannot be maintained, and the XPM-induced frequency shift will stagnate. In our example, new components are originally created by self-phase modulation of the dispersive wave. The initial chirp then conveys these segments into the interaction zone.

For a negative chirp, the spectrum of the dispersive wave initially appears broadened as some material dispersion is pre-compensated. Nevertheless, this initial phase is followed by spectral narrowing. In turn, this leads to deterioration of the matching condition already during the first collision process, resulting in a slower acceleration process.

At further increase or decrease of the initial chirp, temporal reshaping of the dispersive wave becomes dominant. This situation is considered in the next section.

4 Effect of strongly chirped dispersive waves on the collision process

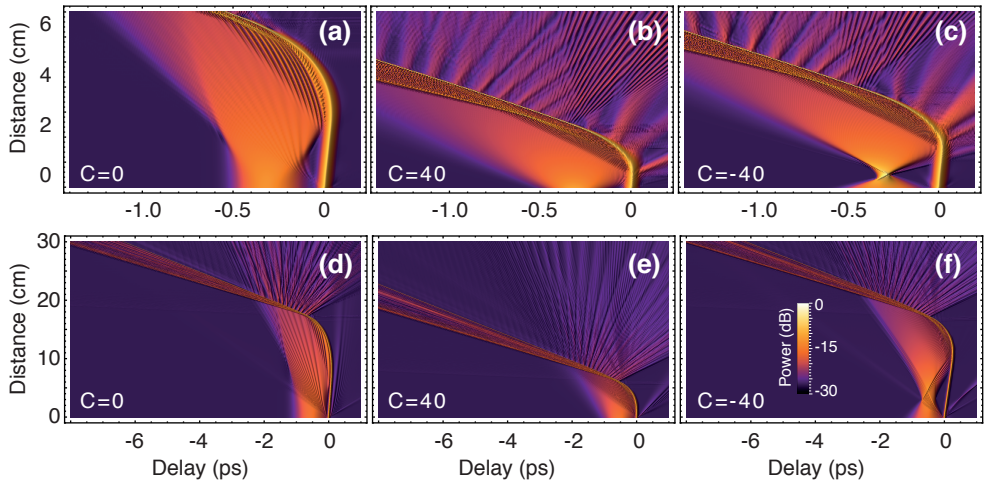

Figure 3: Temporal dynamics of a soliton interacting with a resonant chirped dispersive wave for (a-c) $t_d = 100$ fs, $t_0 = 300$ fs, $\mathcal{E}_d = 0.6\mathcal{E}_s$ and (d-f) $t_d = 300$ fs, $t_0 = 500$ fs, $\mathcal{E}_d = 0.4\mathcal{E}_s$ for different input chirps C of the dispersive wave. Soliton parameters and the initial delay as in Fig. 2.

When propagating through the fiber, a chirped dispersive wave experiences shaping different from an unchirped one, to the end of varying amplitude upon initial contact with the soliton. For the collision process, this results in a simultaneous change of parameters that

influence the collision process. Here we focus on the situation where maximum compression is achieved, i.e., even without an initial chirp, the chosen parameters enable practically ideal compression [1]. Quite generally, the chirp does not allow any further compression beyond the ideal result of a single-cycle pulse, yet may enable restoration of the ideal situation in case of disturbing effects like the Raman effect. Let us nevertheless first explore, how an additional chirp on the dispersive wave actually affects the adiabatic soliton compression process.

Figure 3 depicts the collision process in the time domain with and without initial chirp of the dispersive wave for two different pulse width combinations. Apart from the chirp C value, Figs. 3 (a)-(c) are based on identical soliton and dispersive wave parameters as utilized in Fig. 2. The case without a chirp ($C = 0$) is shown in Fig. 3(a) and is identical to the scenario in Fig. 2(a). With a positive chirp of $C = 40$ [GDD $\approx 250\,\mathrm{fs}^2$, Fig. 3(b)], the initial temporal broadening of the dispersive wave is enhanced, so that the first collision process appears earlier in the propagation. Apart from spectral broadening due to the initial chirp, a broader temporal background of dispersive radiation is created, enabling a longer interaction zone with the soliton. In this way, a stronger total acceleration of the soliton results, which then translates into enhanced adiabatic compression of the soliton. Applying a negative chirp parameter [$C = -40$, GDD $\approx -250\,\mathrm{fs}^2$ in Fig. 2(b)], the dispersive wave is initially compressed until its chirp is compensated. Further dispersive broadening then creates background radiation that again enables interaction with the soliton over extended distances. In the collision process, the amplitude of the dispersive wave is larger than without an initially chirped pulse. The increased amplitude then leads to a stronger acceleration of the soliton for both signs of the chirp parameter C. As the amplitude is the most efficient control parameter of this all-optical manipulation scheme [2, 1], small amplitude variations of the dispersive wave may already strongly affect the soliton acceleration process.

In summary, exploiting temporal reshaping, a strong initial chirp can be used as an alternative way to simultaneously adjust the dispersive wave duration and time delay. However, chirp and delay are not perfectly equivalent control parameters. Because of the nonlinear effects discussed in the previous section, introducing a chirp to a dispersive wave is not completely equivalent to the changing the delay between the soliton and the dispersive wave.

In Figs. 3(d)-(f), we depict the corresponding collision process for a soliton and a dispersive pulse with the width of $t_d = 100\,\mathrm{fs}$, delay of $t_0 = 300\,\mathrm{fs}$ and $\mathcal{E}_d = 0.6\mathcal{E}_s$. These pulse parameters correspond to a scenario where one reaches already the absolute limitation of spectral broadening for the soliton. Initially, the soliton is adiabatically compressed up to a point where it falls abruptly into a state with lower peak intensity and broader pulse width. These limitations are inherent for this compression scheme and ultimately enforced by the spectral boundaries dictated by the ZDW and the on-set of absorption [1]. One particular consequence is the incapability of increasing the compression factor solely by the chirp, as is illustrated in Fig. 4. Here the dynamics of the soliton maximum is shown for different chirps, both for short [Fig. 4(a)] and for long [Fig. 4(b)] pulses. As can be seen, the maximum intensity remains nearly the same, although it is achieved at different propagation lengths z. The electric field of the soliton and dispersive waves at different stages of propagation are shown in Figs. 4(c-h). At the end of the fiber, we receive a cycle number N_c below two. N_c has been calculated at FWHM of the corresponding intensity profile of a soliton. Nevertheless, the strength of the acceleration can indeed be controlled, which enables the compression on shorter propagation distances (see for example red lines in Fig. 4). In this way, the chirp can be used to adapt the compression behavior to the available length of the fiber. This means of control is particularly useful when the point of maximum compression is already observed

at very short distances. As we show in the following, the chirp-induced control becomes even more important when the Raman effect has to be compensated.

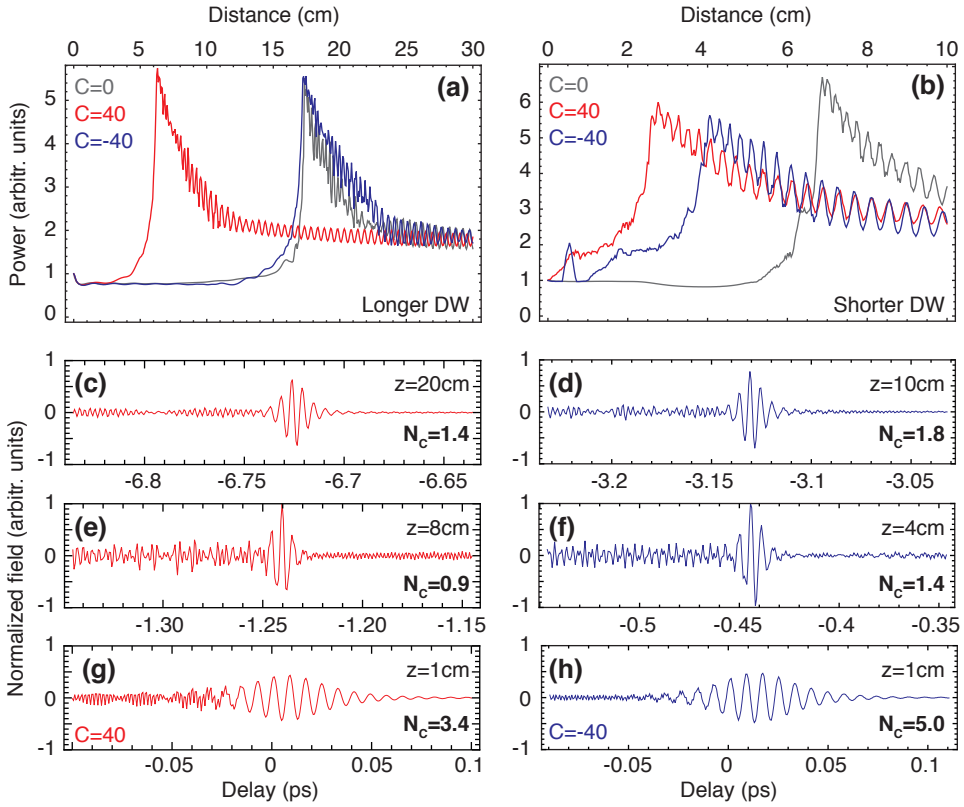

Figure 4: Evolution of the soliton maximum with z for $t_d = 300$ fs (a) and $t_d = 100$ fs (b) for different input chirps C of the dispersive wave and other parameters as in Fig. 2. Electric field of the soliton and the dispersive wave at the (c,d) end, (e,f) the point of maximum compression, (g,h) at an early propagation stage in the fiber for the evolutions shown in (a) and (b), respectively. N_c in (c-h) represents the cycle width of the soliton.

5 Chirped dispersive waves for cancellation of the Raman soliton self frequency shift

So far, we have excluded the Raman effect in our considerations. In fact, the Raman effect does not exclude the collision process [8, 4, 14], but requires a more careful selection of the initial pulse parameters [21, 22] to obtain similar results for the pulse compression as without the Raman effect. In particular, the soliton-self-frequency shift has to be taken into account for the group-velocity matching of dispersive wave. The first collision process has to be realized in such a way that the red shift induced by the Raman effect is compensated. Upon further propagation, the induced blue-shift has to overcome the soliton-self-frequency-shift in order to obtain an effective adiabatic soliton compression. The initial parameters have to be chosen suitably to ensure that the amplitude of the radiation is sufficient to continuously induce a frequency shift of the soliton into the blue during the entire interaction process. Only the low

intensity parts of the dispersive wave interact with the soliton, and the intensity and the width of the initial dispersive wave ensure the build-up of a low level background from broadening of the dispersive wave. At higher intensities of the DW, it mostly crosses the soliton, with only a small interacting part remaining. Nevertheless, the intensity of the dispersive wave at the collision point has to be high enough for compensating any counteracting deceleration induced by the Raman self-frequency shift. This condition naturally implies that the group velocities of both pulses be not too close to each other, limiting the range of the resonant condition for the reflection process.

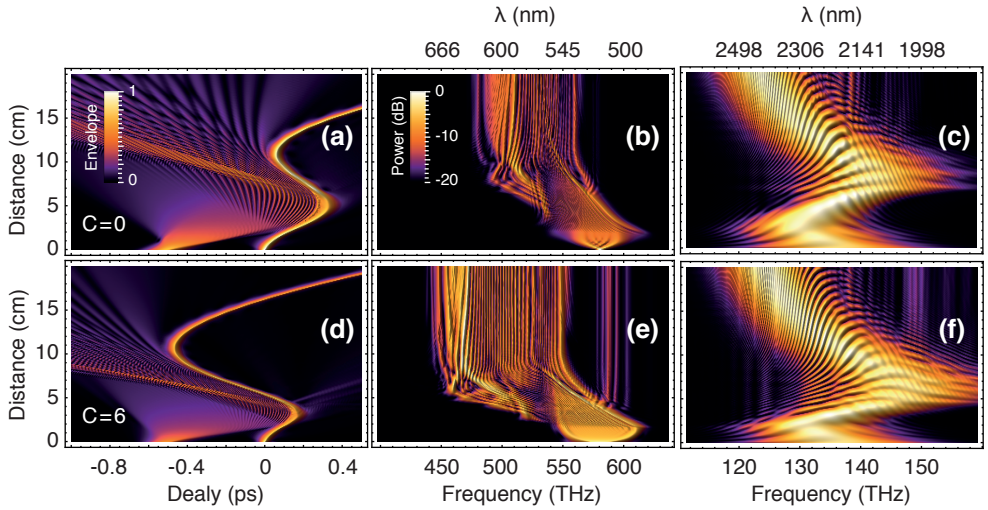

Figure 5: Dynamics of soliton and dispersive wave interaction in the temporal (a,d) and spectral (b,c,e,f) domain taking into account the Raman process for $C = 0$ (a-c) and $C = 6$ (GDD $\approx 1620\,\mathrm{fs}^2$) (d-f). (b,e) Spectral evolution of soliton and (c,f) of dispersive wave.

Figure 5 shows the collision process under the influence of the Raman effect. During the collision the soliton-self-frequency shift is canceled over propagation distances during the collision stage. At a certain point, the interaction between the dispersive wave and the soliton ceases to support sufficiently strong acceleration of the soliton, and the soliton self-frequency shift subsequently determines the soliton trajectory. In turn, the soliton is shifted back towards the red, which then leads to broadening and deceleration of the soliton. In contrast to the Raman-free case, an adjusted interaction length is now essential for the formation of a compressed soliton at the fiber output.

Finally, the presence of the chirp may serve to enhance the interaction length, leading to a stronger compression of the soliton. This is exemplified in Fig. 6, where the behavior of the soliton maximum is shown for different chirp factors as well as for different amplitudes of the dispersive wave. Obviously, in the presence of Raman effect, the compressing factor due to interaction with the dispersive wave is less than in the case without Raman. For low amplitudes of the dispersive wave, even a simple re-compression may be impossible to achieve. Nevertheless, the presence of a chirp in the dispersive wave can improve the situation (see Fig. 6(a)). On the other hand, when a relatively high recompression ratio is achieved (see Fig. 6(b), the chirp is not likely to improve the compression. The comparison of Fig. 5(c,d) shows that the spectral dynamics of the dispersive wave is significantly different in the case with and without chirp. In particular, a low-frequency part of the dispersive wave appears

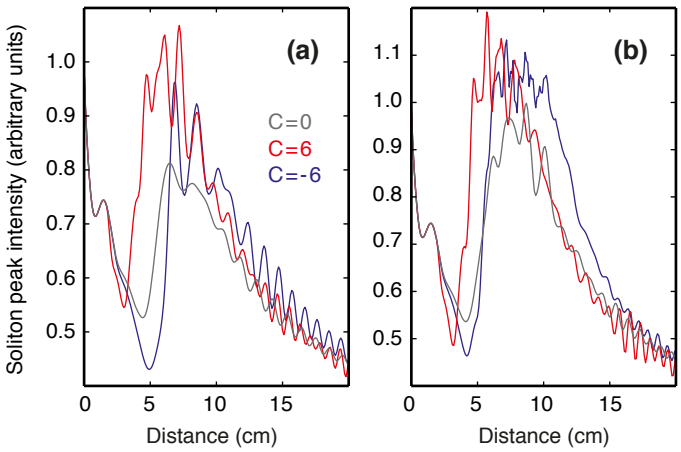

Figure 6: Evolution of the soliton maximum with z for $\mathcal{E}_d = 0.67\mathcal{E}_s$ (a) and $\mathcal{E}_d = 0.75\mathcal{E}_s$ (b) for different input chirps C ($C = 0$: grey line, $C = 6$: red line, $C = -6$ (GDD $= -40000\,\mathrm{fs}^2$): blue line) of the dispersive wave and other parameters as in Fig. 2 and $t_d = 500$ fs.

much more pronounced in the case with chirp. This clearly shows once more that the temporal reshaping of the dispersive wave plays only a minor role in this case. Much more importantly, is the fact that spectral resonance relations between the soliton and dispersive wave are modified by the chirp.

6 Conclusion

In conclusion, we have studied the dynamics of a short soliton resonantly interacting with a chirped dispersive wave packet in an ESM photonic crystal fiber. We found that a relatively small chirp can already significantly modify the dynamics of the interaction process. In general, there are two major mechanisms influencing the dynamics, namely, one related to the phase-matching condition governing the interaction of the soliton and dispersive wave and a second one relating to purely linear reshaping of the chirped dispersive wave in time. The latter mechanism is important for large input chirps and allows controlling the point where dispersive wave and soliton start to interact. On the other hand, the former case allows for an improvement of the soliton-dispersive wave interaction in the spectral domain. This second mechanism relies on spectral broadening of the chirped wave, and it enables a match of the compression behavior to the fiber length. Specifically, one can obtain the maximum soliton compression at shorter propagation distances. Moreover, the chirped dispersive wave is very useful for the control of the soliton compression process in presence of the Raman effect. This means of control provides an additional independent degree of freedom, enabling the modification of time and position of the first collision. In particular, introduction of a positive chirp reduces this time and provides longer interaction distances. The outlined mechanisms enable substantial adaption of the adiabatic soliton compression to a given dispersion characteristics of the fiber. Moreover, the demonstrated control exploits the working principle of an optical transistor for the control of the width and compression factor of a soliton, yielding a controllable and transient pulse compression.

We gratefully acknowledge support by The Einstein Center for Mathematics Berlin under

project D-OT2 and the Collaborative Research Center 123 PlanOS

References

[1] A. Demircan, Sh. Amiranashvili, C. Brée, U. Morgner, and G. Steinmeyer, "Adjustable pulse compression scheme for generation of few-cycle pulses in the midinfrared," Opt. Lett. **39**, 2735-2738 (2014).

[2] A. Demircan, Sh. Amiranashvili, and G. Steinmeyer, "Controlling light by light with an optical event horizon," Phys. Rev. Lett. **106**, 163901 (2011).

[3] D. V. Skryabin and A. V. Gorbach, "Colloquium: Looking at a soliton through the prism of optical supercontinuum," Rev. Mod. Phys. **82**, 1287 (2010).

[4] A. V. Gorbach and D. V. Skryabin, "Bouncing of a dispersive pulse on an accelerating soliton and stepwise frequency conversion in optical fibers", Opt. Express, **15**, 14560 (2008).

[5] A. V. Yulin, D. V. Skryabin, and P. St. J. Russell, "Four-wave mixing of linear waves and solitons in fibers with higher-order dispersion," Opt. Lett. **29**, 2411–2413 (2004).

[6] C.M. De Sterke, "Optical push broom", Opt. Lett. **17**, 914-916 (1992).

[7] N. G. R. Broderick, D. Taverner, D. J. Richardson, M. Ibsen, and R. I. Laming, "Optical Pulse Compression in Fiber Bragg Gratings," Phys. Rev. Lett. **79**, 4566–4569 (1997).

[8] T.G. Philbin, C. Kuklewicz, S. Robertson, S. Hill, F. Konig, and U. Leonhardt, "Fiber-Optical Analog of the Event Horizon," Science, **319**, 1367–1370 (2008).

[9] D. Faccio,"Laser pulse analogues for gravity and analogue Hawking radiation," Cont. Phys., **53**, 97–112 (2012).

[10] K. E. Webb, M. Erkintalo, Y. Xu, N. G. R. Broderick, J. M. Dudley, G. Genty, and S. G. Murdoch, "Nonlinear optics of fibre event horizons," Nature Commun. **5**, 4969 (2014).

[11] R. Smith, "Reflection of short gravity waves on a non-uniform current," Math. Proc. Camb. Phil. Soc. **78**, 517–525 (1975).

[12] R. Driben, F. Mitschke, and N. Zhavoronkov, "Cascaded interactions between Raman induced solitons and dispersive waves in photonic crystal fibers at the advanced stage of supercontinuum generation," Opt. Exp. **18**, 25993 (2010).

[13] A. Demircan, Sh. Amiranashvili, C. Brée, C. Mahnke, F. Mitschke, and G. Steinmeyer, "Rogue events in the group velocity horizon," Sci. Rep. **2**, 850 (2012).

[14] A. Demircan, Sh. Amiranashvili, C. Brée, C. Mahnke, F. Mitschke, and G. Steinmeyer, "Rogue wave formation by accelerated solitons at an optical event horizon," Appl. Phys. B **155**, 343–354 (2013).

[15] L. Tartara, "Frequency shifting of femtosecond pulses by reflection at solitons," IEEE J. Quantum Electron. **48**, 1439–1442 (2012).

[16] R. Driben and I. Babushkin, "Accelerated rogue waves generated by soliton fusion at the advanced stage of supercontinuum formation in photonic-crystal fibers," Opt. Lett. **24**, 5157–5159 (2012).

[17] R. Driben, A. V. Yulin, A. Efimov, and B. A. Malomed, "Trapping of light in solitonic cavities and its role in the supercontinuum generation," Opt. Express **21**, 19091–19093 (2013).

[18] A. V. Yulin, R. Driben, B. A. Malomed, and D. V. Skryabin,"Soliton interaction mediated by cascaded four wave mixing with dispersive waves," Opt. Express **21**, 14481–14486 (2013).

[19] S. Batz and U. Peschel, "Diametrically driven self-accelerating pulses in a photonic crystal fiber," Phys. Rev. Lett. **110**, 193901 (2013).

[20] M. Wimmer, A. Regensburger, C. Bersch, M.-A. Miri, S. Batz, G. Onishchukov, D. N. Christodoulides, and U. Peschel, "Optical diametric drive acceleration via action-reaction symmetry breaking," Nature Phys. **9**, 780–784 (2013).

[21] A. Demircan, Sh. Amiranashvili, C. Brée, and G. Steinmeyer, "Compressible octave spanning supercontinuum generation by two-pulsen collisions," Phys. Rev. Lett. **110**, 233901(2013).

[22] A. Demircan, Sh. Amiranashvili, C. Brée, U. Morgner, and G. Steinmeyer, "Supercontinuum generation by multiple scatterings at a group velocity horizon," Opt. Express **22**, 3866–3879 (2014).

[23] L. Tartara, "Soliton control by a weak dispersive pulse," J. Opt. Soc. Am. B **32**, 395 (2015).

[24] J.M. Stone and J.C. Knight, "Visibly 'white' light generation in uniform photonic crystal fiber using a microchip laser", Opt. Express **16**, 2670 (2008).

[25] C. Agger, C. Petersen, S. Dupont, H. Steffensen, J. K. Lyngs, C. L. Thomsen, J. Thgersen, S. R. Keiding, and O. Bang, "Supercontinuum generation in ZBLAN fibers — detailed comparison between measurement and simulation," J. Opt. Soc. Am. B, **29**, 635 (2012).

[26] T. Balciunas, C. Fourcade-Dutin, G. Fan, T. Witting, A. A. Voronin, A.M. Zheltikov, F. Gerome, G.G. Paulus, A. Baltuska and F. Benabid, "A strong-field driver in the single-cycle regime based on self-compression in a kagome fibre," Nature Commun. **6**, 6117 (2015).

[27] S.V. Chernikov, D.J. Richardson, D.N. Payne, and E.M. Dianov, "Soliton pulse compression in dispersion-decreasing fiber," Opt. Lett. **18**, 476–478 (1993).

[28] D. Gabor, "Theory of communication," J. Instit. Electr. Eng. **93**, 429 (1946).

[29] M. Born and E. Wolf, "Principles of Optics", Cambridge University Press, 7th edition, (1999).

[30] Sh. Amiranashvili and A. Demircan, "Hamiltonian structure of propagation equations for ultrashort optical pulses," Phys. Rev. A **82**, 013812 (2010).